Technical Report

TR-2011-013

Automatic neck plane detection and 3D geometric characterization of aneurysmal sacs

by

Marina Piccinelli, Yiemeng Hoi, David Steinman, Alessandro Veneziani, Luca Antiga

Mathematics and Computer Science

EMORY UNIVERSITY

Automatic neck plane detection and 3D geometric characterization of aneurysmal sacs

Marina Piccinelli[1] Yiemeng Hoi[2] David Steinman[2]

Alessandro Veneziani[1] Luca Antiga[3,4]

1 - Department of Mathematics and Computer Science, Emory University, Atlanta, US

2 - Department of Mechanical and Industrial Engineering, University Of Toronto, Toronto, Canada

3 - Orobix srl, Bergamo, Italy

4 - Department Of Bioengineering, Mario Negri Institute, Bergamo, Italy

Abstract

Geometric indices defined on intracranial aneurysms have been widely used in rupture risk assessment and surgical planning. However, most indices employed in clinical settings are currently evaluated based on two-dimensional images that inevitably fail to capture the three-dimensional nature of complex aneurysmal shapes. In addition, since measurements are performed manually, they can suffer from poor inter and intra operator repeatability. The purpose of the current work is to introduce objective and robust techniques for the 3D characterization of intracranial aneurysms, while preserving a close connection to the way aneurysms are currently characterized in clinical settings.

Techniques for automatically identifying the neck plane, key aneurysm dimensions, shape factors, and orientations relative to the parent vessel are demonstrated in a population of 15 sidewall and 15 terminal aneurysms whose surface has been obtained by both level-set segmentation and thresholding by two trained operators. Neck plane location and geometric indices obtained with our techniques are in very good agreement both between level set segmentation and thresholding and between operators. By capturing the 3D nature of aneurysmal sacs and by minimizing observer variability, our approach allows large retrospective and prospective studies on aneurysm geometric risk factors to be performed using routinely acquired clinical images.

Keywords: cerebral aneurysms, morphology, geometry, neck section automatic identification, 3D geometry and morphology quantification

1. Introduction

Intracranial aneurysm rupture is a catastrophic clinical event that often leads to subarachnoid hemorrhage and is associated with significant morbidity and mortality. In recent years, the increased rate of detection of unruptured aneurysms has presented clinicians with the major dilemma on whether to treat incidentally discovered aneurysms or conservatively monitor them. Since surgical procedures carry their own intrinsic risks, the ideal situation would be to address only those lesions that are more likely at risk of rupture, yet no robust and reliable method is available to estimate the specific risk of rupture for a given aneurysm.

In common clinical practice, size, shape and location are the most widely used factors to assess an aneurysm's rupture risk and accordingly plan a treatment. Size characterization is traditionally carried out by means of straight-line measurements, often performed manually on two-dimensional (2D) angiographic views. Among these, height is commonly defined as the maximum perpendicular distance of the dome to the plane defining the neck[17,18,20,24] and sac maximum diameter as the largest cross sectional diameter along the height[10,17,20,24,33]. Aneurysm shape is also considered to play a crucial role in rupture: possible means of shape characterization range from a qualitative classification into simple-lobed versus multi-lobular aneurysms[20,26] to ratios between dimensions of interest[13,29]. For instance, aspect ratio[30], defined as aneurysm height to neck width, and bottleneck factor[13], as the sac maximum diameter over the neck diameter, stand as the most widely tested among them. However, the reliability of these

simple and/or descriptive parameters in predicting rupture risk and the lack of agreement in the definition of critical dimensions have generated much controversy and, even if introduced as a straightforward approach to cope with the complex three dimensional (3D) nature of aneurysm geometry, their very simplicity may actually overlook potentially decisive 3D features of the shape of intracranial aneurysms.

Technological advances in imaging modalities, such as three dimensional rotational angiography (3D-RA), have indeed improved our ability in describing aneurysms in 3D and have consequently allowed the quantification of more sophisticated geometrical and morphological indices that may correlate with aneurysm rupture status. Besides volumes and areas, made accessible by 3D reconstruction techniques of aneurysm surface models, the most investigated parameters include wall undulation factor, non-sphericity and ellipticity indexes, conicity parameter[10,24,33], as well as relations between 2D and 3D features, such as the volume-to-ostium ratio[26,31]. Recently, parent vasculature geometry and its spatial relationship with aneurysm dome have also been associated with rupture status: the size ratio index, that requires the extraction of the maximum aneurysm height - hence of the neck plane - and of the parent vessel radius has shown a strong correlation with rupture[10,18]; geometric features such as torsion and curvature have been investigated for both idealized and realistic geometries[14,22]; angles of inclination of aneurysm sac and parent vessel with respect to neck plane have been proposed as additional morphological metrics with varying degrees of success[4,10,11]; clustering of patients based on parent vessel features has been performed with a functional principal component analysis of geometric data[27].

A major issue concerning the assessment of aneurysm geometry and morphology is

the lack of standardization or consensus on how measurements should be defined on 3D models once these are reconstructed from imaging data. No widely accepted definitions of aneurysm constituents are available, such as neck or sac, which makes it difficult to design objective methods to delineate them and unfeasible to compare results between different studies or clinical trials, especially given the heterogeneity of aneurysms shapes and configurations. In particular, the identification of the neck is a decisive step on which all subsequent operations for geometric characterization rely upon. Delineation of the neck has mostly been performed manually on 2D views or interactively in 3D[10,16,17], and relies on visual observation and observers' expertise rather than on a standardized definition. Recently, Cardenes et al[5], Larrabide et al[15] and Ford et al[12] have defined a strategy for the isolation of the aneurysm sac using curved boundaries, based respectively on model local surface characteristics, on the analysis of the topology of vasculature skeletons and on parent vessel reconstruction, from which a definition of neck plane can be inferred. On the other hand, objective techniques for a rigorous, quantitative description of shape and size of aneurysms that remains adherent to their 3D nature are still lacking. Specifically, shape indices mainly rely on straight-line measurements that are straightforward to obtain, either manually or using automated procedures, but inevitably provide a crude first-order approximation of the geometry for complex aneurysmal shapes, potentially impacting on their discriminant power.

The purpose of the current work is two-fold. First, we demonstrate an automated technique for the identification of the aneurysm neck plane in 3D and the isolation of the aneurysm sac from its parent vasculature. Second, we introduce a framework of objective geometric criteria for the 3D characterization of intracranial aneurysms in order to obtain,

where possible, fully 3D correlates of currently used 2D or straight-line indices. We then demonstrate the applicability of our definitions to patient-specific geometries and their robustness to segmentation techniques and operators on a population of lateral and terminal aneurysms obtained from 3D-RA. A visual and quantitative comparison of geometric and morphological indices suggested in this work to analogous parameters commonly found in literature is also presented.

2. Materials and Methods

2.1 Overview

The proposed methodology for 3D characterization of aneurysmal sacs consists of two successive steps. First, the aneurysm is isolated from its parent vasculature using a novel and automated approach for defining the aneurysm neck. Second, a set of indices describing the morphology of the isolated aneurysm sac and the parent vasculature are computed. The approach relies on the concepts of Voronoi Diagram (VD), centerline extraction and tube function as described in [1, 21] and on their implementation within the Vascular Modeling Toolkit (VMTK)[2], an open source project for vascular modeling.

2.2 Datasets

The *Aneurisk* surface models database was employed to develop the algorithms presented and test their efficacy and reliability. *Aneurisk* (2005-2008) was a research project for the development of geometric, biomechanical and statistical tools for the analysis of cerebral aneurysms. The database contains aneurysms from 153 consecutive patients who underwent 3D-RA for cerebral aneurysm assessment at the Niguarda

Hospital in Milan, Italy according to clinical routine between 2002 and 2006. Images were obtained with an Integris Allura Unit (Philips, The Netherlands; 55 deg/s, 512x512 matrix, 25 frames) after the injection of 18 ml of contrast agent at 4 ml/s and were reviewed by a senior radiologist who provided information on rupture status. Radiological images were completely anonymized at the clinical site and then made available in DICOM format for the subsequent analysis.

For the present work, a subset of 30 saccular aneurysm cases (15 sidewall and 15 terminal) was randomly selected from the entire cohort of the Aneurisk database. The only pre-requisite for an aneurysm to be considered admissible for the present study was the presence of a long enough portion of parent vasculature (at least 4 radii away from the lesion), so to allow a correct reconstruction of the parent artery without the aneurysm; giant aneurysms, given their size, are commonly treated irrespective of their geometry, and were consequently not included in the study. Ultimately, the 30 cases selected for the study included 18 aneurysms developing along the Internal Carotid Artery (ICA), 6 occurring at the Anterior Communicating Artery (ACA) bifurcation and 6 along the Middle Cerebral Artery (MCA). Twelve aneurysms were diagnosed as ruptured at the time of scanning, 18 as unruptured.

The selected cohort was segmented independently by two trained operators using the segmentation tool provided within VMTK[2], based on a gradient-driven level-set approach. Particular attention was paid so that the largest possible portion of the acquired vasculature was included in the final models. In the following, we will refer to these two sets of segmented models as LS1 and LS2. Since the most immediate 3D reconstruction technique adopted in clinical settings is image thresholding, two additional sets of

surfaces were generated by thresholding the original 3D-RA images by the same two operators, with sufficient time after level set segmentation so as to effectively blind the operators. The criterion for thresholding the images was to find the best approximation of the lumen surface for both the aneurysmal sac and its nearby vasculature. This operation was in some cases challenging since image quality, inhomogeneity of contrast agent, large size of aneurysms and the presence of contiguous structures in the region of interest interfered in obtaining clean surface models. In the following we will refer to the sets of thresholded model as TH1 and TH2.

2.3 Automatic extraction of aneurysmal sac surface and identification of neck cross section

Extraction of the sac surface

The first step for the automatic isolation of the surface of the aneurysm sac and identification of the neck is the approximation of the parent vasculature at the aneurysm site by means of an automatic algorithm for aneurysm digital removal[12]. As an additional output of the aneurysm removal procedure, the extent of the area of influence of the aneurysm on the parent vasculature is provided as locations on the vessels centerlines. In the following paragraphs we will refer to these locations as clipping points. Figure 1(a) depicts the original 3D surface and the reconstructed parent vasculature for one sidewall. We refer to the cited paper [12] for all technical details about the aneurysm removal technique.

Once the parent vasculature has been reconstructed, the identification of the aneurysm sac is obtained by virtual subtraction of the reconstructed parent vasculature from the

original surface model. From a technical point of view, the aneurysm sac is extracted by making use of the definition of centerlines and *tube functions*[1,21]. The centerline of the reconstructed parent vasculature is first considered and its tube function is defined as the union of the maximal inscribed spheres centered at the centerline points. Formally, this requires the evaluation of the following expression for a generic point **x** in R^3

$$T_{c,r}(\mathbf{x}) = \min_{s} [\, | \mathbf{x} - \mathbf{c}(s)|^2 - r^2(s)] \qquad (1)$$

where s the parametric coordinate traveling along the centerline, **c** a generic centerline point and r the corresponding maximal inscribed sphere radius. The zero iso-surface of the tube function (1) for a vascular segment identifies the *tube surface*, a surface strictly contained into the vessel and characterized by a varying radius and a circular cross section. By evaluating the difference between the reconstructed parent vessel tube function and the Voronoi diagram spheres falling outside the reconstructed tube, every point on the original surface (prior to aneurysm removal) is associated to a positive (negative) value indicating whether the point lies on the aneurysm or on the parent vessel (Figure 1(b)). Clipping the original surface model at the zero level of the tube function difference allows the isolation of the aneurysmal surface from the model. This surface exhibits a curved boundary that may be strongly wrapped around the local parent vessels, in relation to how aneurysm growth has affected the shape of the parent vasculature (Figure 1(c)).

Identification of aneurysm neck cross section

For the identification of the aneurysm neck, the distance of each point on the isolated aneurysmal surface to the reconstructed parent vessel between the clipping points is

initially computed, i.e. the distance of each sac point to the tube lying just beneath the aneurysm. This operation is performed similarly to aneurysmal surface extraction by evaluating the tube function of the parent vasculature centerline between the clipping points for all aneurysmal surface points. Isocontours of the hence generated distance field at increasing values of distance define sets of surface curves that move away from the parent artery and over the aneurysm dome in a way that reflects the 3D shape of the aneurysm sac and parent vascular structures and their relative orientation. The barycenters of a fine set of such isocontours are then fitted with a cubic spline to generate a reference line through the aneurysm neck and sac (Figure 1(d-e)).

The aneurysmal surface is then sliced with a plane at each spline point first perpendicularly to the spline and, successively, with an array of planes regularly precessing around the reference line. Resorting to spherical coordinates terminology, the orientation of each slicing plane can be described in terms of inclination and azimuth angles: the inclination angle defines the tilting of the plane with respect to the tangent to the reference line, while the azimuth angle defines the amount of rotation around the reference line. The actual slicing is performed for inclination angles ranging from 0 to 30 degrees with a step of 2 degrees, and azimuth angles spanning the 360 degrees at interval of 10 degrees. Figure 1(e) depicts some of the planes cutting the surface for one location along the reference line.

For each slice of the sac surface, the algorithm tests whether an open or closed profile is generated, given the saddle shape of the aneurysmal surface at the interface with the parent artery: if the section is closed, its area is calculated. Following this approach, the aneurysm neck section is defined as the first closed section for which the area has a local

minimum, which is expected to correspond to the section through which the aneurysm inflow is most concentrated.

Once the neck cross section has been identified, the final aneurysm sac is isolated from the 3D original surface along the corresponding plane direction (Figure 1(f)).

2.4 3D geometric characterization of the aneurysm sac and its parent vasculature

After the aneurysm sac has been objectively isolated, its morphological characterization can be addressed. On the basis of some of the geometric concepts detailed in the previous paragraphs, a set of measurements and related indices for the 3D characterization of the morphology of the aneurysm sac and its relationship to the parent vasculature will be presented in the next sections. The parameters are listed according to the structure they aim to describe, namely aneurysm sac, neck section, parent vasculature and relative position and orientation between aneurysm sac and parent vasculature.

2.4.1 Aneurysm sac shape approximations and size characterization

Voronoi Diagram envelopes and centerlines

The shape of the aneurysm sac is effectively described by means of the VD and its envelope. The VD is a geometric entity that allows the derivation of its originating surface through the envelope of all the maximal inscribed spheres centered at its vertices[1,21]. In that, the VD provides a compact geometric description of a generic shape. Figure 2(a) depicts two extreme situations: an aneurysm with a near-spherical shape and a lobulated one; the VD structure is shown inside the aneurysm sac.

From the VD we derive a novel descriptor of aneurysm shape, the *Voronoi Diagram*

Core (VDC), defined as the portion of the VD whose vertices are associated to a radius greater than 75% of the maximum Voronoi radius in the sac. Its envelope represents a smaller portion of the complete sac volume, encompassing the most stable, essential features of the aneurysm shape. Evidently, the heavier the pruning of VD vertices in the definition of the VDC, the more regular the resulting shape of its envelope. The threshold of 75% of the maximum Voronoi radius was empirically chosen as a reasonable compromise between the search of shape simplification on one hand and need of capturing the essential aneurysm shape on the other.

The VDC is not influenced by surface irregularities or the presence of blebs and daughter sacs. Figure 2(b) illustrates how the VDC envelope recovers nearly the whole aneurysm sac volume in case of aneurysms with a regular shape, while for lobulated aneurysms the VDC envelope accounts for the most regular portion of the sac. Given the envelope surfaces, volume and surface area estimates are readily provided.

Based on the VD and the VDC, a robust definition of the *sac centerline* can also be introduced, with the rationale of measuring the 3D length of the aneurysm by not constraining the measurement to a straight line, but allowing it to follow the main aneurysm shape as identified by the VDC. First, the outermost point of the centerline is determined as the furthest point from the ostium barycenter over the VDC (obtained solving the eikonal equation over the VDC[21] with initial values at the neck plane) and for which the maximal sphere radius is the largest. Successively, the sac centerline is computed over the complete VD having the outer location and the ostium barycenter respectively as target and source points. Being computed from the neck barycenter to the outmost point on the VDC, the sac centerline stays medial within the sac and travels

along its most stable medial structures without being influenced by the presence of daughter sacs. As the centerline doesn't touch the surface (since the VD is at a distance of at least one sphere radius from it), the actual sac length is finally obtained adding to the computed centerline length the radius of the maximal inscribed sphere centered at its most distal point. In Figure 2(c) the sac centerline and its last maximal inscribed sphere is shown for two differently shaped aneurysms.

As an additional characterization of the sac dimensions, its *largest cross section* is identified by slicing the aneurysm sac using planes perpendicular to the VDC centerline and simply selecting the section with the largest area (Figure 2(c)).

Inscribed ellipsoid and semi-axes

In addition to the VDC envelope, a further abstraction of the aneurysm shape is achieved by means of the *inscribed ellipsoid* that best fits the aneurysmal sac. The advantage of adopting an inscribed ellipsoid as opposed to a least square fit ellipsoid as proposed in [25] is that the latter suffers from the presence of blebs and surface irregularities and for this reason it may not align with aneurysm the main directions. The inscribed ellipsoid geometric primitive provides us with linear and volumetric measures of the main portion of the aneurysm morphology in terms of the semi-axes and the ellipsoid volume. Although the ellipsoid can not account for the entire sac complex features, its semi-axes, specifically the maximum and minimum values, here referred to as *saxis1* and *saxis3*, and their ratio may be a useful first order index for the categorization of aneurysm shapes, from mainly spherical to prolate or oblate ellipsoids, as recently proposed in [25] (Figure 2(d)).

2.4.2 Aneurysm neck section characterization

From the definition of the neck plane, identified in the previous sections, the *ostium area* is readily measurable. In addition, to quantitatively characterize the deviation of the section shape from that of a perfect circle, the minimum and maximum ostium size are extracted, referred to as *min* and *max ostium size*, respectively.

2.4.3 Parent vasculature characterization

The most immediate characterization of the geometry of parent vessels is their radius, which is directly accessible after centerline extraction, according to [21]. Given the presence of the aneurysm, a reliable estimate of vessel size should be close to the aneurysm but not under its influence, since aneurysm growth may have altered the local vascular morphology. A reliable location for vessel size measurement is at the clipping points, as defined previously in the context of aneurysm isolation. In order to make such measurement more robust to spurious local surface features, vessel radii are estimated as the average radius over an interval of one maximal inscribed sphere radius starting at the clipping point and moving away from the aneurysm. In Figure 3(a), clipping point positions and the corresponding intervals are shown for one lateral and one terminal aneurysm. Similarly to schemes proposed in [10], a concise measure of the vessels diameter was designed. For lateral aneurysms this consists in the averaged value at the clipping point upstream the aneurysm location, while for terminal ones a further averaging step is performed to account for the dimensions of all vessels meeting at the aneurysm site[10].

2.4.4 Relative 3D orientations between aneurysm, neck plane, parent vessels

Spatial relationships, specifically the relative orientations and angles existing between the sac, the neck and parent vessel are regarded as important aspects to investigate for an exhaustive characterization of aneurysms, as recently underlined in [10, 18]. To this end, three unit vectors are introduced to concisely describe the position of the above mentioned structures, namely $\mathbf{u}_{sac}$, $\mathbf{u}_{neck}$, $\mathbf{u}_{vessel}$. From the VDC centerline, the sac unit vector $\mathbf{u}_{sac}$ is defined as the direction of the straight line connecting the neck barycenter to the most distal centerline point. The neck unit vector $\mathbf{u}_{neck}$ is the normal to the neck section, which is directly available from the extraction of the neck plane itself. The parent vessel unit vector $\mathbf{u}_{vessel}$ is retrieved as the direction of the tangent vector to the centerline at the upstream clipping point for lateral aneurysms and at the common branch clipping point for terminal ones.

Correct calculation of angles between directions in 3D requires the definition of a common plane onto which the vectors should first be projected and angles between projected vectors measured. Following the approach described in [10] where a "*viewing plane [...] that captures the incoming flow entering*" an aneurysm is chosen in order to quantify the aneurysm inclination and the vessel angles, an analogous plane is automatically identified from vessel centerlines by means of the bifurcation plane as defined in [1, 21]. This is straightforward for terminal aneurysms, where the required bifurcation plane is defined from the parent vessel centerlines, while for sidewall configurations the aneurysm bifurcation plane is employed, as introduced in [22]. The following angles are measured between the projected unit vectors: the angle between the

aneurysm sac and the vessel, $\theta_{sac\text{-}vessel}$ and the angle between neck section plane and the vessel, $\theta_{neck\ -\ vessel}$. In Figure 3(b and c), the three unit vectors and their projections on the aneurysm plane are depicted for a sidewall and a terminal aneurysm.

2.5 Derived geometric indices

On the basis of the geometric definitions introduced in the previous sections, derived morphological indexes can be computed. Such indices are constructed to reflect those currently used in clinical and research settings, at the same time being defined in 3D and relying on robust criteria. The result is the design of geometrical and morphological parameters that are either 3D analogues of existing indexes or that represent new indices for the characterization of sac dimensions and shape made possible by the 3D nature of our evaluations. Specifically, the following indexes are here computed: aspect ratio, AR[30], size ratio, SR[10,18], bottleneck factor[13], ellipsoid axes ratio[25] and two formulations for the recently introduced volume-to-ostium ratio[26,31].

Differently from common definitions, aspect ratio and size ratio are computed using the sac centerline length as a measure of aneurysm sac height, i.e. the length of the most stable portion of the aneurysm shape measured from the ostium barycenter plus the last maximal inscribed sphere radius (Fig 2(c)). The bottleneck factor, traditionally computed in 2D as the ratio between linear measurements, sac largest diameter over neck diameter, is obtained as the ratio between the largest sac section area to the ostium area. Similarly to the methodology proposed in [25], according to which the essential morphology of the sac can be derived as ratios between three major perpendicular sizes manually measured on angiograms, we here define an analogous shape index as the ratio of saxis3 over

saxis1 obtained from the inscribed ellipsoid. Finally, the sac volume-to-ostium area ratio is computed according to the usual formula, as well as in a modified version where the volume of the VDC envelop is employed instead, leading to the *core volume-to-ostium area ratio*.

2.6 Algorithm performance and statistical analysis

To evaluate the efficacy and the reproducibility of the algorithms for the identification of the neck cross section and the isolation of the aneurysm sac, their performance on all cases of datasets LS1 and TH1 was qualitatively evaluated and compared.

Consistency and reproducibility of the morphological indices were quantified by means of the Interclass Correlation Coefficient (ICC). The ICC, ranging from 0 to 1, is commonly employed to assess agreement in measurements performed by multiple observers, 1 indicating perfect agreement, 0 largest discrepancy[32]. Specifically all indices were tested for inter-observer and inter-modality (i.e. level set segmentation versus thresholding) consistency by comparing results obtained on the four datasets, LS1,2 and TH1,2.

Finally, as an additional evaluation, indices on segmented models LS1 and LS2 were considered as ground truth and the relative errors of corresponding measurements performed on datasets TH1 and TH2 were evaluated by direct comparison.

All statistical analyses were performed using the R statistical package[23].

2.7 Extraction of straight-line measurements and related parameters

In previous work (Ma et al[17], Raghavan et al[24], Dhar et al[10]), morphological indices

had been presented largely based on straight-line measurements. Such indices were then tested for their statistical significance in assessing association with rupture[10,18,33,24]. In those works, straight-line measurements were carried out automatically, but only after the neck plane had been manually determined. The automated neck plane identification introduced in the present work allows to apply these measurements in a fully automated and objective fashion.

In order to provide a comprehensive comparison between straight-line measurements and the ones proposed in the present work, the following quantities were also computed after the neck has been identified and the sac isolated according to our automatic approach: maximum perpendicular height[17], maximum cross-sectional area along the height (from which the sac maximum diameter estimate is determined[17]), maximum aneurysm height[10], and surface area and volume of the aneurysm convex hull[17]. In addition, derived parameters were computed, namely undulation index[24], ellipticity index[24], non-sphericity index[24], aspect ratio[30] (maximum perpendicular height over neck diameter) and bottleneck factor[13] (ratio of sac maximum equivalent diameter over neck diameter). The measurements were performed by following the algorithmic details and the formulas given in the cited papers.

The conventional parameters were also tested on the four datasets LS1,2 and TH1,2 for consistency and reliability by means of the ICC. In addition, visual comparisons with respect to analogous indices proposed in the present work are presented, namely heights vs sac centerline, maximum cross sectional areas based on perpendicular height vs sac centerline, convex hull shape vs VDC envelope.

3. Results

Identification of ostium cross section and extraction of sac surface

As shown in Figure 4 for the entire cohort of models, our technique for the identification of the ostium cross section and the isolation of the aneurysmal sac produced plausible results for all cases. Algorithms were indeed stable for both terminal and lateral configurations and different shapes, sizes and orientations of the sac with respect to the parent vessels. The neck detected according to our automated approach is localized at the interface between parent vessel and aneurysm sac and did not necessarily retrieve the absolute narrowest cross section, a feature that actually allowed the identification of a reasonable neck section also for sidewall wide neck aneurysms, or for aneurysms that did not present a narrowing in the proximal portion of the sac. Similarly, in terminal cases, this approach localized the neck cross section just above the origin of the daughter arteries, thus isolating the aneurysm sac exactly where the influence of the parent vasculature could reasonably be considered negligible.

The corresponding thresholded models obtained by the first operator (TH1) are shown in Figure 5 for visual assessment of the reproducibility of results. Even for rather rough surface meshes our definition of the neck section provided reasonable results. When these results are compared to those obtained on more robustly segmented models (LS1), the overall positioning of necks for each pair of 3D surfaces can be considered consistent, considering the actual differences determined by threshold selection.

Extraction of geometric parameters

In Table 1, geometric parameters are detailed according to the structure they are meant

to describe, namely ostium section, parent vessels, aneurysm sac, aneurysm sac core, spatial orientations. A specific category is dedicated to derived indices, for a total of 21 indexes analyzed. Given the substantial difference in 3D configuration between sidewall and terminal aneurysms, the description of angulation of aneurysm and neck with respect to parent vasculature are reported separately. Descriptive statistics for all variables relative to the four datasets is reported, to account for the overall features of the data under study, their dispersion and the general agreement in the measurements among different segmentation techniques and different operators. For each analyzed variable. minimum, maximum, mean and standard deviations are listed.

In order to specifically test the reproducibility of the characterization in Table 2, ICCs between different reconstruction techniques or inter-operators were evaluated for each index; further, relative errors were computed to investigate the accuracy of the measurements obtained from the thresholded subsets TH1 and TH2 with respect to those performed on the segmented models LS1 and LS2, here considered as ground truth.

As detailed in Table 2, excellent agreement was found for the majority of the computed parameters, as indicated by ICC $\geq$ 0.90.This is particularly true for the inter-operator comparisons, i.e. LS1 vs LS2 and TH1 vs TH2, for which reproducibility was near-perfect, and in particular for parameters characterizing the ostium section, the aneurysmal sac and its core dimensions (ICC $\geq$ 0.95).

Furthermore, intra-modality comparisons, i.e. LS1 vs TH1 and LS2 vs TH2, exhibited excellent agreement. Analogously to the previous case, the most reliable results were found for ostium, sac and sac core indexes quantifications.

For both inter-modality and inter-operator comparisons the poorest values of ICC were

found for indexes characterizing the angulation of aneurysm sac and neck section with respect to the closest parent vessel direction. While they may still be considered acceptable for the inter-operator accordance (ICC ~ 0.80), they revealed a few small values in the inter-modality analysis (ICC < 0.60). Analogously, some of the derived variables obtained as ratios of linear measurements, in particular the ellipsoid axes ratio, showed to be more dependent on the surface reconstruction modality.

When inter-operator agreements obtained for the two surface reconstruction techniques were compared, no statistically significant differences were found (p-value = 0.39). The same holds true for the two sets of inter-modality coefficients obtained by the two operators (p-value = 0.42).

By considering the level-set segmented surface models as ground truth, the accuracy of measurements on thresholded models was evaluated. With the exception of angulation indexes, relative differences never exceeded 20%. Consistent with the reproducibility test, smallest values were obtained on average for indices describing the neck ostium, the sac and the core dimensions, while higher relative differences were emphasized for the orientation indices, further underlying the sensitivity of these geometric parameters to surface reconstruction techniques.

Extraction of straight-line measurements and related parameters

Figure 6 and 7 (Additional Material) show a visual comparison between the definitions proposed in the present work and those based on straight-line measurements. Essential geometric features are shown comparatively in the 30 cases of the LS1 dataset, namely maximum perpendicular and maximum aneurysm heights vs sac centerline path,

positions and orientations of maximum cross sectional areas, and surface irregularities through convex hull vs the VDC. For a quantitative comparison, Table 3 reports numerical values for the geometric parameters for each case depicted in Figures 6 and 7. Interestingly, maximum aneurysm height and sac centerline identify a consistent direction for aneurysms with simpler shapes, although the sac centerline tends to more closely reflect local surface features. For irregular shapes, the discrepancy between straight-line and centerline-based measurements can be significant, as in cases 19 and 22. Cases 31 to 33, still belonging to the Aneurisk database but not included in the 30 randomly selected cases, are reported here to further corroborate this observation.

Similarly to Tables 1 and 2, Tables 4 and 5 report the descriptive statistics of straight-line-based measurements performed on the 4 datasets, the ICCs and relative errors to evaluate their inter-segmentation modality and inter-operator robustness and accuracy. These results show that direct measurements (height, surface area and volume) exhibit good or very good agreement, while the derived parameters, particularly regarding the undulation index, are generally less robust. Overall the relative errors stay within the range described for our newly introduced parameters, with the exception of indices involving the convex hull, that may be strongly influenced by surface irregularities resulting from thresholding operations.

4. Discussion

The robust isolation of the aneurysmal sac and the rigorous characterization of its morphology are operations of primary importance in the study of cerebral aneurysms, with potential implications for rupture risk stratification, surgical planning and

investigations on the relationships between geometry and hemodynamics.

In this work, we first introduced newly developed algorithms for the automatic detection of the aneurysm neck plane and the isolation of the aneurysmal sac from the parent vasculature. We then introduced a new set of objective criteria that allow a 3D automated characterization of geometry and morphology of the aneurysm sac and a generalization of traditional measurements, which are usually achieved on 2D projections or evaluated in 3D using straight-line measurements once the aneurysm neck plane has been interactively defined.

The ultimate goal of the present work was to propose robust, operator-independent methods for a full 3D characterization of the morphology of the aneurysm sac, while retaining a compatibility with existing, clinically validated measurements.

Identification of neck cross section and isolation of aneurysm sac

Robust delineation of the aneurysm neck has proven to be a challenging albeit fundamental task for the characterization of aneurysms, mostly due to a lack of standardized definitions and the high variability in aneurysm shapes and configurations. In many important works[10,16,17] on sac geometry characterization, the neck plane is manually identified on radiological images or 3D surfaces as the plane where the aneurysm pouches outward from the parent vessel. Recently, valuable efforts have been devoted to automate this step: *Cardenes et al*[5] proposed a technique for the automatic localization of the neck on 3D surfaces whereby the neck is defined as a smooth curve located at the transition between the aneurysm and the tubular part of the vessel and separates the sac from the healthy portion of the feeding arteries. According to their

technique, the line identifying the neck is directly computed over the surface as a minimal action path and results in a non-planar 3D curve around the neck. In *Larrabide et al*[15], the neck is also first automatically identified as a non-planar 3D curve, but successively approximated with an averaged planar section from which linear geometric measurements of the aneurysm sac are performed. While manual and automated approaches appear as two different and alternative ways of defining the neck - as a single plane along which the sac is isolated from the parent vasculature or as a non-planar 3D curve that carves the aneurysm sac following local surface features[5,28] - these two approaches provide complementary information and strongly relate to the actual goal of sac isolation. While, as pointed out in [5], a non-planar 3D curve better isolates the aneurysm sac in complex configurations or situations with highly deformed parent vessels, the definition of a neck plane is necessary in many applications, from the computation of geometric indices such as ostium area, neck diameter and sac height, to endovascular treatment planning[3], to quantitative characterization of hemodynamics[7,8,19]. Treatment of saccular aneurysms with endovascular coiling or surgical clipping often rely on accurate depiction of the neck plane and its relationship to adjacent vessels[3], as well as on ostium dimensions and shape (e.g. circular versus elliptical). In [7], the 3D neck outline is initially delineated directly on surface models by hand, and then a plane is finally obtained for the quantification of hemodynamics features, i.e. inflow rate or velocity distributions at the neck.

The fully-automated techniques presented in this work detect a planar neck section after having identified a 3D curve that separates the aneurysm sac from the parent vasculature. Starting from the approximation of the parent vasculature without

aneurysm[12], we identify a non-planar boundary for the aneurysmal surface at its interface with the parent vessel(s). This a first approximation of the true aneurysm sac that strongly depends on the degree of local deformation that the parent vasculature may have undergone due to the aneurysm growth. From there, we identify a planar cross section as the aneurysm neck which allows the robust separation of the aneurysm sac from its parent vasculature by means of a single planar cut. We argue that deriving the aneurysm plane as a simple planar approximation of the curved aneurysm boundary would not have resulted in a similar robustness due to the high dependence of such curved boundary from the degree of involvement of the parent vessel during the aneurysm development process.

As demonstrated throughout the paper, our approach can be robustly applied to a variety of aneurysm sizes, shapes and locations. In addition, it is robust to surface quality and largely insensitive to surface segmentation methods. These advantages open the door to fast, reliable and systematic approach to the detection of the aneurysm neck, all essential requisites to large clinical studies, routine clinical use and robust geometric characterization.

3D morphological characterization of aneurysmal sac and parent vasculature

Use of radiological modalities such as 3D-RA, CTA or MRA and technological developments in reconstruction and visualization have indeed improved our ability in displaying and consequently acknowledging the complex 3D morphology of cerebral aneurysms, which supposedly plays a crucial role in aneurysm evaluation and strongly influences treatment planning (e.g. clipping, coiling and stenting). Nevertheless, tools and methodologies for a robust geometric characterization of anatomical structures, including

blood vessels, in 3D are still quite limited. Raghavan et al[24] introduced a set of parameters and indexes to account for the 3D shape of aneurysms, such as undulation index, non-sphericity index and ellipticity index, by combining various approximations of sac volume. In Chien et al[9], a minimal bounding sphere was constructed around the aneurysm sac and the ratio of aneurysm volume to sphere volume computed in order to reflect the 3D shape of the sac. Towards a similar end, we here proposed two different approximations of the aneurysmal sac: the VDC envelope and the inscribed ellipsoid. The VDC envelope represents by construction the most stable portion of the aneurysm sac shape from which blebs and daughter sacs are excluded, with the rationale of identifying the most hemodynamically "active" portion of the sac, where primary aneurysmal flow patters are expected to develop. Since the VDC envelope only accounts for regular portions of the aneurysm shape, a comparison between VDC envelope and the original sac volume provides a direct measure of sac irregularity. A quantitative index categorizing irregularly shaped aneurysms may be helpful in testing the generally accepted notion that these types of aneurysms are more likely to rupture because of concentration hemodynamic stresses occurring at blebs[6]. Previously proposed indices for the quantification of surface irregularities are provided by the convex hull volume and surface area (e.g. undulation and ellipticity index[10,17,24]). Figure 7 (Additional Material) shows the convex hull and the VDC envelope compared to the true aneurysm sac for the LS1 dataset. In contrast to the convex hull, the VDC is strictly located inside the sac and it is less influenced by the presence surface irregularities, which might stem from segmentation artifacts. This might explain the lower reliability of convex hull-derived measurements compared to VDC-based ones.

The inscribed ellipsoid also constitutes a stable, albeit poorer, subset of the aneurysmal volume; the advantageous feature of this representation is the possibility of expressing its dimensions in terms of the semi-axes and their ratio. The ratio between ellipsoid semi-axes is similar to the indices proposed by *Raghavan et al*. in [25], as first order approximations of aneurysm shape, The automatic nature of the calculation of our index makes it more suitable for large-scale population studies.

Next to aneurysm "size", the most commonly employed, single linear measurement of aneurysm size in clinical and research settings is aneurysm height. Different definitions and implementations of this parameter have been given in recent years, namely the maximum distance or the maximum perpendicular distance from the neck plane[10,17,18,20] and the neck barycenter position. Being extracted as straight lines, these measurements essentially quantify the aneurysm 'length' on a some projection, i.e. without accounting for the actual spatial development of the sac in 3D. A novel linear measurement of aneurysm size, the sac centerline, was therefore proposed. Its path is computed directly in 3D and it is oriented in the direction of the VDC, which confers greater stability to the measurement when compared to straight-line measurements. Being based on maximum distances over the sac, the latter can in fact be influenced by the presence of blebs and daughter sacs, as well as by segmentation artifacts. As graphically shown in Figure 6 (Additional Material), this can make a difference for the more irregularly shaped aneurysms and can have a marked effect on the orientation of the section from which maximal sac diameter and area are computed. This has a direct effect on the computation of the bottleneck factor, which here relies on slicing the sac perpendicularly to the computed sac centerline instead of along directions parallel to the neck plane. Figure 6

and Table 3 (Additional Material) show the difference in the positioning of the largest section and in the value of its area between centerline-based and maximum perpendicular height-based methods, and how the former tend to more closely reflect the local orientation of the sac.

A natural extension of the aspect ratio to 3D - volume over area, rather then a ratio between linear measurements - is provided by the volume-to-ostium area ratio, as a surrogate measure of sluggish flow within the sac. In addition to this standard definition, we also proposed a novel core-volume-to-ostium area ratio, which excludes daughter sacs and blebs, where blood flow is expected to be very slow, from the volume estimate.

Last, an approach for objectively characterizing the relative positioning between anatomical structures, such as between the neck plane and the main sac direction, has been proposed. This information has a direct relevance in clinical settings - the orientation of the neck with respect to parent vessels may impact the ability to effectively coil or clip an aneurysm - as well as in the search for geometric surrogates of intra-aneurysmal hemodynamics, such as the prediction of impingement regions or inflow jets, with implications on the definition of a rupture risk.

5. Conclusions

In this work, we presented a framework of fully automated methods for a fully 3D characterization of the shape of intracranial aneurysms, which directly extends previously introduced 2D and 3D straight-line measurements which have undergone clinical validation throughout the years.

As part of the present work, we demonstrated the reliability of our techniques on a

population of lateral and terminal aneurysms whose surfaces have been obtained with different methods (level sets vs thresholding) and by two different operators. Our definitions have shown to yield remarkably reproducible values for the computed indices and have led to very similar neck plane positions and orientations, both in inter-modality and inter-operator comparisons, even in cases where thresholding produced noisy surfaces including artifactual structures in proximity to and over the aneurysm.

While the concepts introduced in this work represent a technical advancement with respect to the current practice, the clinical significance of the resulting indices and their ability in providing insights into the disease mechanisms and/or improving the design of reliable rupture risk indices have to be extensively investigated. In this context, the automated nature of our techniques allows their application to large scale explorative studies, clinical trials and clinical routine. Towards the same end, we have chosen to make the implementation of the methods presented in this paper available as part of the open-source VMTK project, with the goal of promoting the adoption of 3D measurements in clinical and research settings, encouraging the development of new measurements based on the introduced geometric constructions and increasing the reproducibility and comparability of results from population studies on the prediction of aneurysmal outcomes and the planning of adequate treatment strategies.

6. Acknowledgements

This study was supported by by a grant from the Canadian Institutes of Health Research. YH and DAS also acknowledge the support of, respectively, a Research Fellowship and Career Investigator Award from the Heart & Stroke Foundation of

Canada. Aneurisk (2005-2008) was a joint project developed at MOX-Politecnico di Milano for the development of geometric, computational and statistical tools for the analysis of cerebral aneurysms supported by Fondazione Politecnico di Milano and Siemens Medical Solutions Italy. AV also acknowledges the Brain Aneurysm Foundation.

References

1. Antiga L. and Steinman D.A. Robust and objective decomposition and mapping of bifurcating vessels, IEEE Trans Med Imaging. 23:704-13,2004.
2. Antiga L. and Steinman D.A. Vascular Modeling Toolkit. Available at http://www.vmtk.org.
3. Anxionnat R., Bracard S., Ducrocq X., Trousset Y., Launay L., Kerrien E., Braun M., Vaillant R., Scomazzoni F., Lebedinsky A. and Picard L. Intracranial aneurysms: clinical value of 3D digital subtraction angiography in the therapeutic decision and endovascular treatment. Radiology. 218:799-808, 2001.
4. Baharoglu M.I., Schirmer C.M., Hoit D.A., Gao B.L. and Malek A.M. Aneurysm inflow-angle as a discriminant for rupture in sidewall cerebral aneurysms. Stroke. 41:1423-30, 2010.
5. Cardenes R., Pozo J., Bogunovic H., Larrabide I. and Frangi A. Automatic aneurysm neck detection using surface Voronoi Diagrams. IEEE Trans Med Imag. Published online May 2011.
6. Cebral JR, Sheridan M and Putman CM. Hemodynamics and bleb formation in intracranial aneurysms. AJNR Am J Neuroradiol. 31:304-10, 2010.
7. Cebral J.R., Mut F., Weir J. and Putman C. Quantitative characterization of the hemodynamic environment in ruptured and unruptured brain aneurysms. AJNR Am J Neuroradiol. 32:145-51, 2011.
8. Cebral J.R., Mut F., Weir J. and Putman C.M. Association of hemodynamic characteristics and cerebral aneurysm rupture. AJNR Am J Neuroradiol. 32:264-70,

2011.

9. Chien A., Sayre J. and Vinuela F. Comparative morphological analysis of the geometry of ruptured and unruptured aneurysms. Neurosurgery, Published online Mar 2011.
10. Dhar B.E., Tremmel M., Mocco J., Kim M., Yamamoto J., Siddiqui A.H., Hopkins L.N. and Meng H. Morphology parameters for intracranial aneurysm rupture risk assessment. Neurosurgery. 63:185-96, 2008.
11. Ford M.D., Lee S.W., Lownie S.P., Holdsworth D.W., Steinman D.A. On the effect of parent-aneurysm angle on flow patterns in basilar tip aneurysms: towards a surrogate geometric marker of intra-aneurysmal hemodynamics. 41:241-8, 2008.
12. Ford M.D., Hoi Y., Piccinelli M., Antiga L. and Steinman D.A. An objective approach to digital removal of saccular aneurysms: techniques and applications. Br J Radiol. 82:S55-61, 2009.
13. Hoh B.L., Sistrom C.L., Firment C.S., Fautheree G.L., Velat G.J., Whiting J.H., Reavey-Cantwell J.F. and Lewis S.B. Bottleneck factor and height-width ratio: association with ruptured aneurysms in patients with multiple cerebral aneurysms. Neurosurgery. 61:716-22, 2007.
14. Hoi Y., Meng H., Woodward S.H., Bendok B.R., Hanel R.A., Guterman L.R. and Hopkins L.N. Effects of arterial geometry on aneurysm growth: three-dimensional computational fluid dynamics study. J Neurosurg. 101:676-81, 2004.
15. Larrabide I., Villa-Uriol M.C., Cardenes R., Pozo M.J., Macho J., Roman L.S., Blasco J., Vivas E., Manzo A., Hose D.R. and Frangi A.F. Three dimensional morphological analysis of intracranial aneurysms: A fully automated method for

aneurysm sac isolation and quantification. Med Phys. 38: 2439-49, 2011.

16. Lauric A, Miller EL, Baharoglu MI and Malek AM. 3D shape analysis of intracranial aneurysms using the writhe number as a discriminant for rupture. Ann Biomed Eng. 39:1457-69, 2011.
17. Ma B, Harbaugh R.E. and Raghavan M.L. Three-dimensional geometrical characterization of cerebral aneurysms. Ann Biomed Eng. 32:264-73, 2004.
18. Ma D., Tremmel M., Paluch R.A., Levy E.I., Meng H. and Mocco J. Size ratio for clinical assessment of intracranial aneurysm rupture risk. Neurol Res. 32:482-6, 2010.
19. Mantha A.R., Benndorf G., Hernandez A., Metcalfe R.W. Stability of pulsatile blood flow at the ostium of cerebral aneurysms. Journal of Biomechanics. 42:1081-7, 2009.
20. Parlea L.P., Fahrig R., Holdsworth D.W. and Lownie S.P. An analysis of the geometry of saccular intracranial aneurysms. AJNR Am J Neuroradiol. 20:1079-89, 1999.
21. Piccinelli M., Veneziani A., Steinman D.A., Remuzzi A. and Antiga L. A framework for geometric analysis of vascular structures: application to cerebral aneurysms. IEEE Trans Med Imaging. 28:1141-55, 2009.
22. Piccinelli M., Bacigaluppi S., Boccardi E., Ene-Iordache B., Remuzzi A., Veneziani A. and Antiga L. Geometry of internal carotid artery and recurrent patterns in location, orientation and rupture status of lateral aneurysms: an image-based computational study. Neurosurgery. Published online Jan 2011.
23. R Development Core Team. R: A Language and Environment for Statistical

Computing. Vienna, Austria: R Foundation for Statistical Computing. http://www.R-project.org.

24. Raghavan M.L., Ma B. and Harbaugh R.E. Quantified aneurysm shape and ruptured risk. J Neurosurg. 102:355-62, 2005.

25. Raghavan M.L., Torner J., Zhang J., Meissner I., Piepgras D., Huston J. and Brown R. Assessment of intracranuial aneurysms morphology in a large patient population. 6th World Congress of Biomechanics 2010, Singapore.

26. Ryu C.W., Kwon O.K., Koh J.S. and Kim E.J. Analysis of aneurysm rupture in relation to the geometric indices: aspect ratio, volume, and volume-to-neck ratio. Neuroradiology. Published online Nov 2010.

27. Sangalli M.L., Secchi P., Vantini S., Veneziani A. A case study in exploratory functional data analysis: geometrical features of the internal carotid artery. J Am Stat Assoc. 104:37-48, 2009.

28. Sgouritsa E., Mohamed A., Morsi H., Shaltoni H., Mawad M. and Kakadiaris I. Neck localization and geometry quantification of intracranial aneurysms. IEEE International Symposium on Biomedical Imaging. 1057-60, 2010.

29. Tateshima A., Chien A., Sayre J., Cebral J. and Vinuela F. The effect of aneurysm geometry on the intra-aneurysmal flow condition. Neuroradiology. 52:1135-41 2010.

30. Ujiie H., Tachibana H., Hiramatsu O., Hazel A.L., Matsumoto T., Ogasawara Y., Nakajima H., Hori T., Takakura K. and Kajiya F. Effects of size and shape (aspect ratio) on the hemodynamics of saccular aneurysms: a possible index for surgical treatment of intracranial aneurysms. Neurosurgery. 45:119-29, 1999.

31. Yasuda R., Strother C.M., Taki W., Shinki K., Royalty K., Pulfer K. and Karmonik C. Aneurysm volume-to-ostium area ratio: a parameter useful in discriminating the rupture status of intracranial aneurysms. Neurosurgery. 68:310-7, 2011.

32. Weir J.P. Quantifying test-reliability using the intraclass correlation coefficient and the SEM. Journal of Strength and Conditioning Research. 19:231-240, 2005.

33. Xiang J., Natarajan S.K., Tremmel M., Ma D., Mocco J., Hopkins L.N., Siddiqui A.H., Levy E.I., Meng H. Hemodynamic-morphologic discriminants for intracranial aneurysm rupture. Stroke. 42:144-52, 2011.

Figure 1. Steps for the isolation of the aneurysm sac and the identification of the neck cross section: (a) original 3D surface model (opaque grey) and reconstructed parent vasculature without the aneurysm (red); (b) calculation of the tube function of the reconstructed parent vasculature centerlines on the original model surface; the centerlines tube surface is also shown inside the model; (c) the negative portion of the tube function defined for the reconstructed parent vasculature (light blue surface) identifies the aneurysmal surface over the original surface (in transparency); the zero level of the tube function (light red contour) represents the vessel-sac interface on the surface; (d) distance field to the parent vessel underneath the sac, here identified in terms of its centerline within the clipping points (red), constructed over the aneurysmal surface; the iso-contours of this distance field are shown; (e) the sac reference line obtained by interpolating the barycenters of the distance field iso-contours (red); a set of planes rotating around a centerline point and slicing the sac along different orientations; (f) final isolation of the aneurysm sac after being cut along the plane that identifies the first closed section for which the area has a local minimum.

Figure 2. Geometric approximations and measurements for the aneurysm sac: (a) sac isolation for a near-spherical lateral aneurysm (left) and a terminal lobulated aneurysm (right): the VD structure with the radius of the maximal inscribed spheres (MISR) centered at its points is depicted inside the sac; the VD envelope corresponds to the sac surface (opaque dark grey); (b) for the same cases as in (a) the VDC with its MISR field

is shown inside the sac with its envelope (opaque dark grey) for comparison with the original sac surface (light grey); (c) aneurysm sac centerline extracted over the VDC (opaque dark grey) for an irregular shaped aneurysm (left) and an ellipsoidal one (right); the maximal inscribed sphere at the most distal point of the sac centerline is also shown, whose radius is added to the sac centerline length to obtain the total sac length; the largest cross section along the core centerline is depicted; (d) ellipsoid inscribed into two differently shaped aneurysm sacs.

Figure 3. Geometric characterization of parent vasculature: (a) positions of clipping points and maximal inscribed spheres spheres touching the clipping points for lateral (left) and terminal (right) aneurysms: vessel radius is computed at the upstream position for lateral aneurysms and as the average radius of all parent vessels (common branch and daughter arteries) for terminal ones; isolated sac surface (grey), neck section, three unit vectors $\mathbf{u}_{sac}$, $\mathbf{u}_{neck}$, $\mathbf{u}_{vessel}$, sac centerline, parent vessel centerlines and aneurysm bifurcation plane for a sidewall (b - left) and a terminal aneurysm (c - left); projection of the three unit vectors over the aneurysm plane (b and c right): relative orientations between aneurysm sac and neck section with respect to the direction of the parent vessel are quantified.

Figure 4. Extraction of the aneurysmal surface (dark grey) and the neck plane (red) for the entire cohort of LS1 models. The VDC envelope (red) is also depicted, accounting for the most stable portion of the aneurysms sac shape.

Figure 5. Extraction of the aneurysmal surface (dark grey) and the neck plane (red) for

the entire cohort of TH1 models. The VDC envelope (red) is also depicted, accounting for the most stable portion of the aneurysms sac shape.

Figure 6. Measures of aneurysm sac (light grey) height: straight-line maximum perpendicular distance and maximum aneurysm distance (black) versus sac centerline (white) computed on the VDC (dark grey). The largest sac cross sections are obtained by slicing the aneurysm along the perpendicular (green) and along the sac centerline (red). All the cases from LS1 dataset are shown plus three additional cases taken from the Aneurisk database.

Figure 7. Comparison between convex hull (light grey) and VDC envelope (red) shapes over the aneurysm sac shape (light blue). All the cases from LS1 dataset are shown plus three additional cases taken from the Aneurisk database.

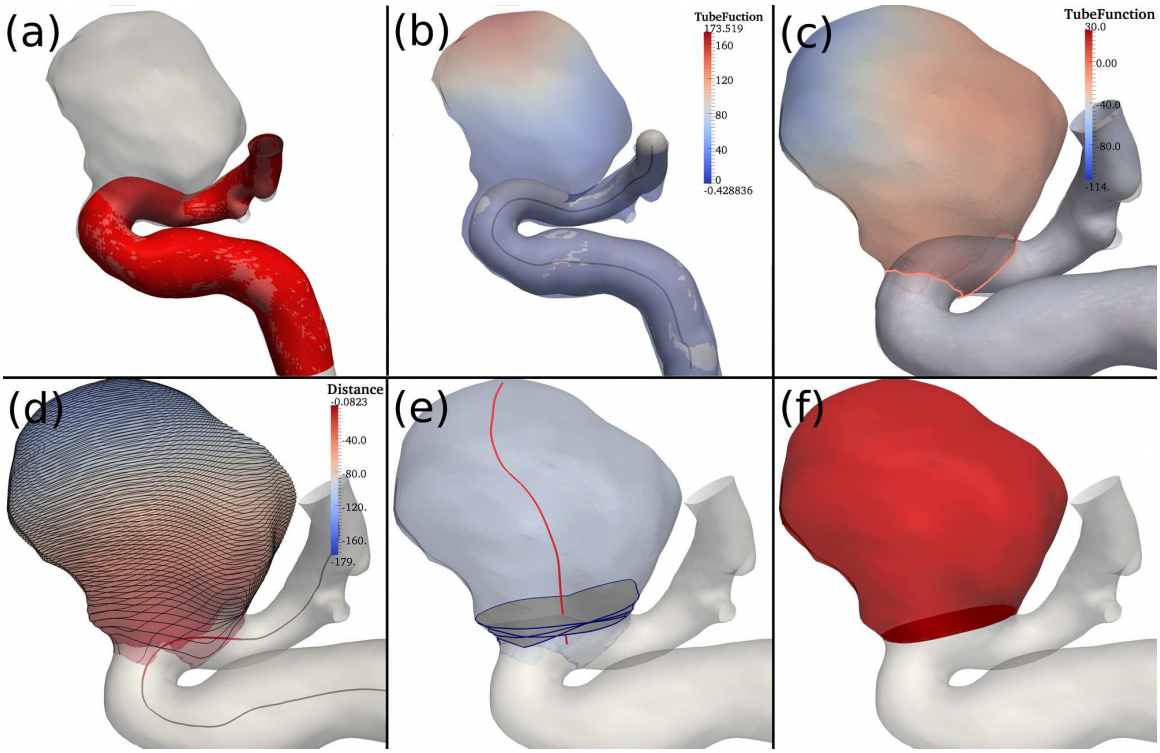
(a)
(b)
TubeFuction
173.519
160
120
80
40
0
-0.428836
(c)
TubeFunction
30.0
0.00
-40.0
-80.0
-114.
(d)
Distance
-0.0823
-40.0
-80.0
-120.
-160.
-179.
(e)
(f)

Figure 1.

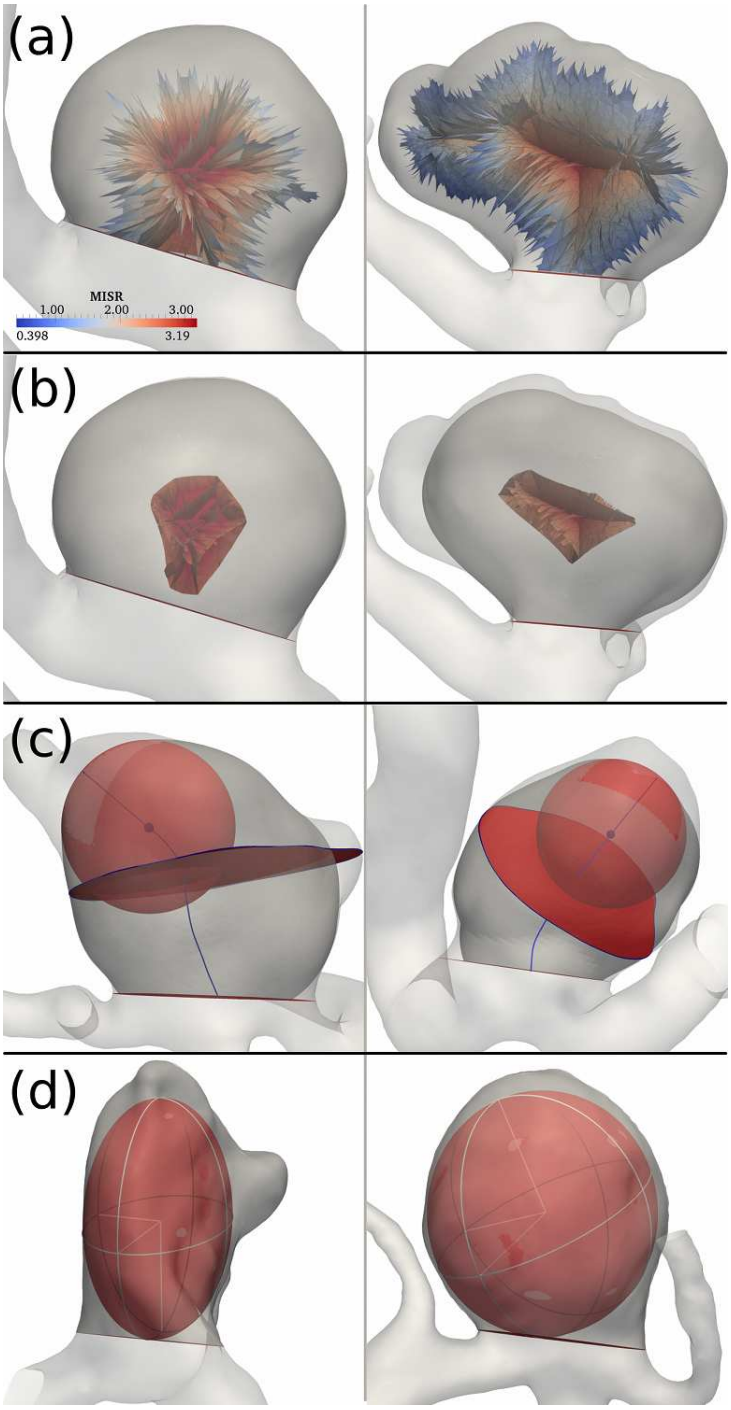

Figure 2.

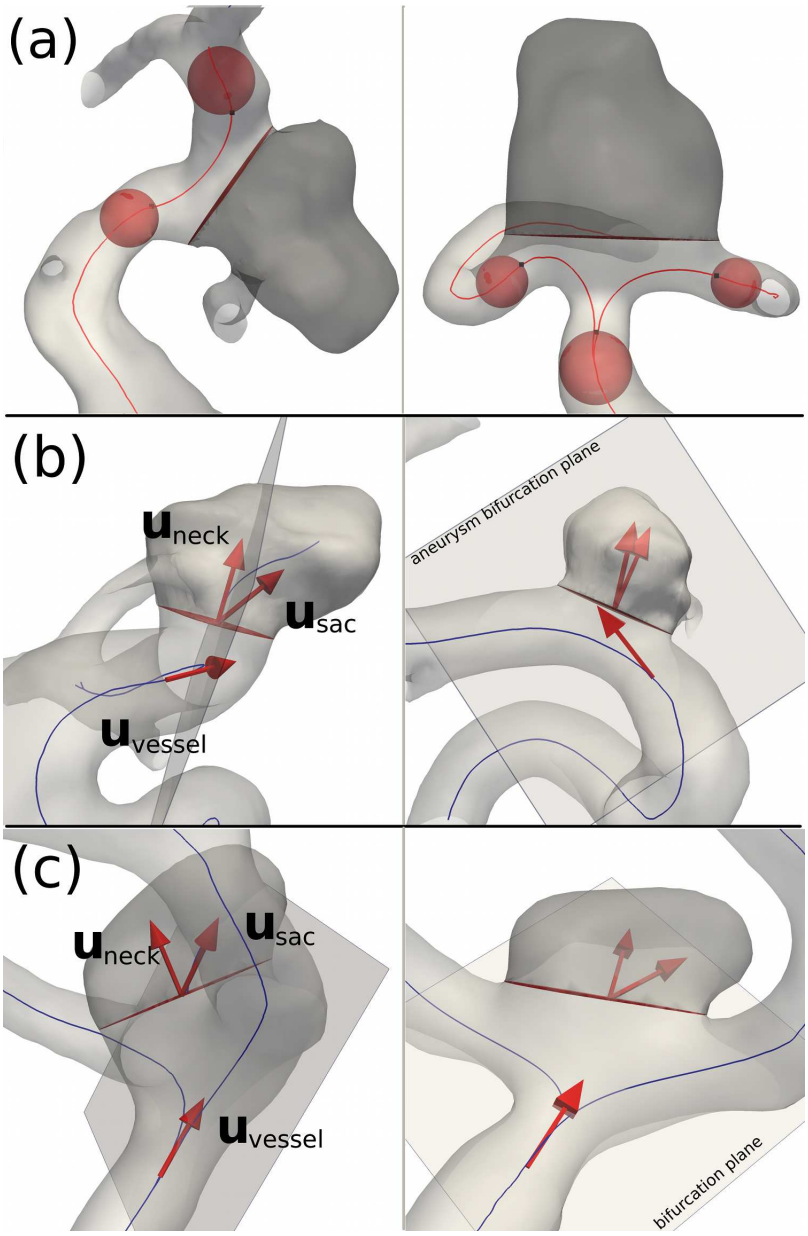
(a)
(b)
$\mathbf{u}_{neck}$
$\mathbf{u}_{sac}$
$\mathbf{u}_{vessel}$
aneurysm bifurcation plane
(c)
$\mathbf{u}_{neck}$
$\mathbf{u}_{sac}$
$\mathbf{u}_{vessel}$
bifurcation plane

Figure 3.

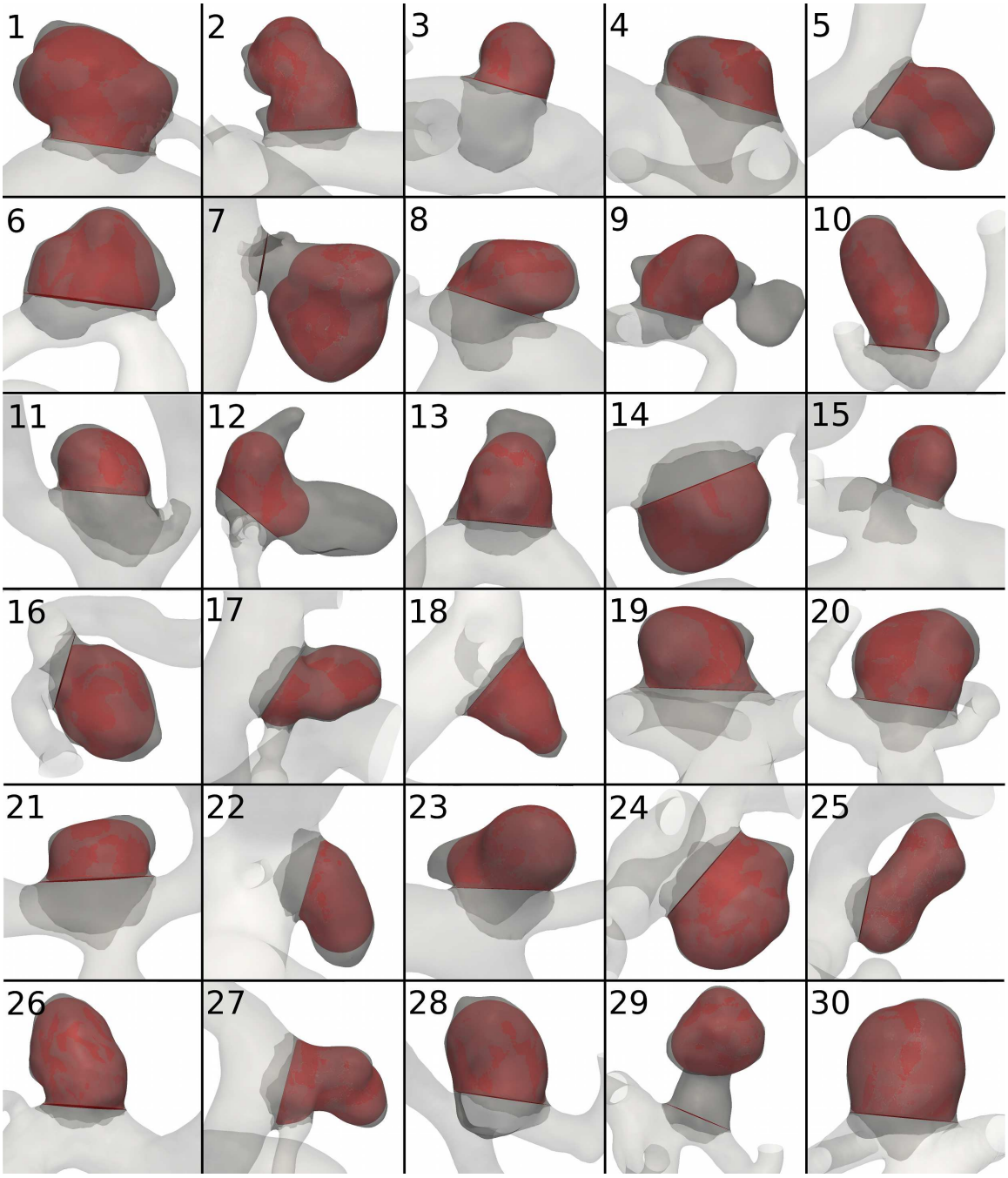
1
2
3
4
5
6
7
8
9
10
11
12
13
14
15
16
17
18
19
20
21
22
23
24
25
26
27
28
29
30

Figure 4.

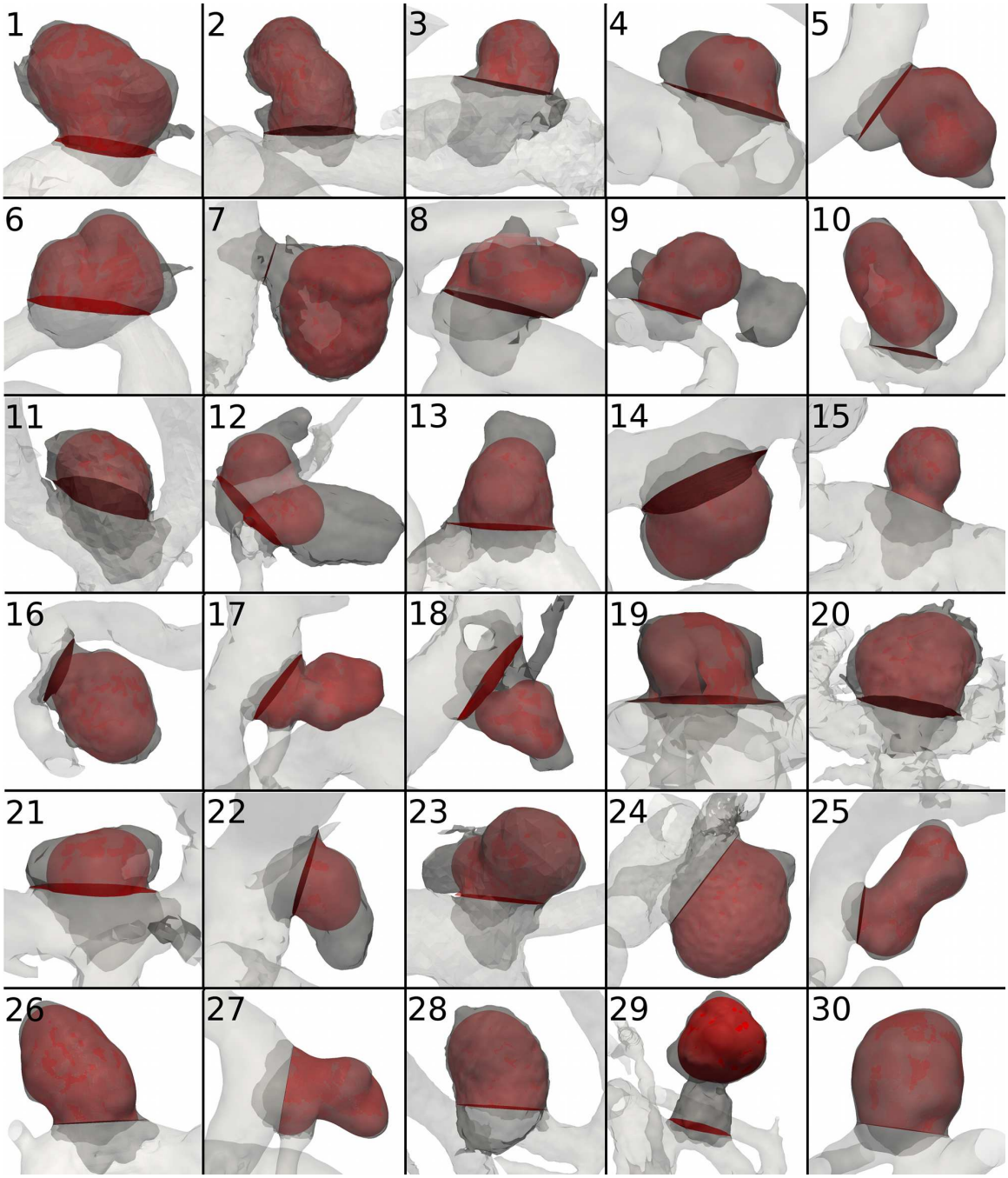
1
2
3
4
5
6
7
8
9
10
11
12
13
14
15
16
17
18
19
20
21
22
23
24
25
26
27
28
29
30

Figure 5.

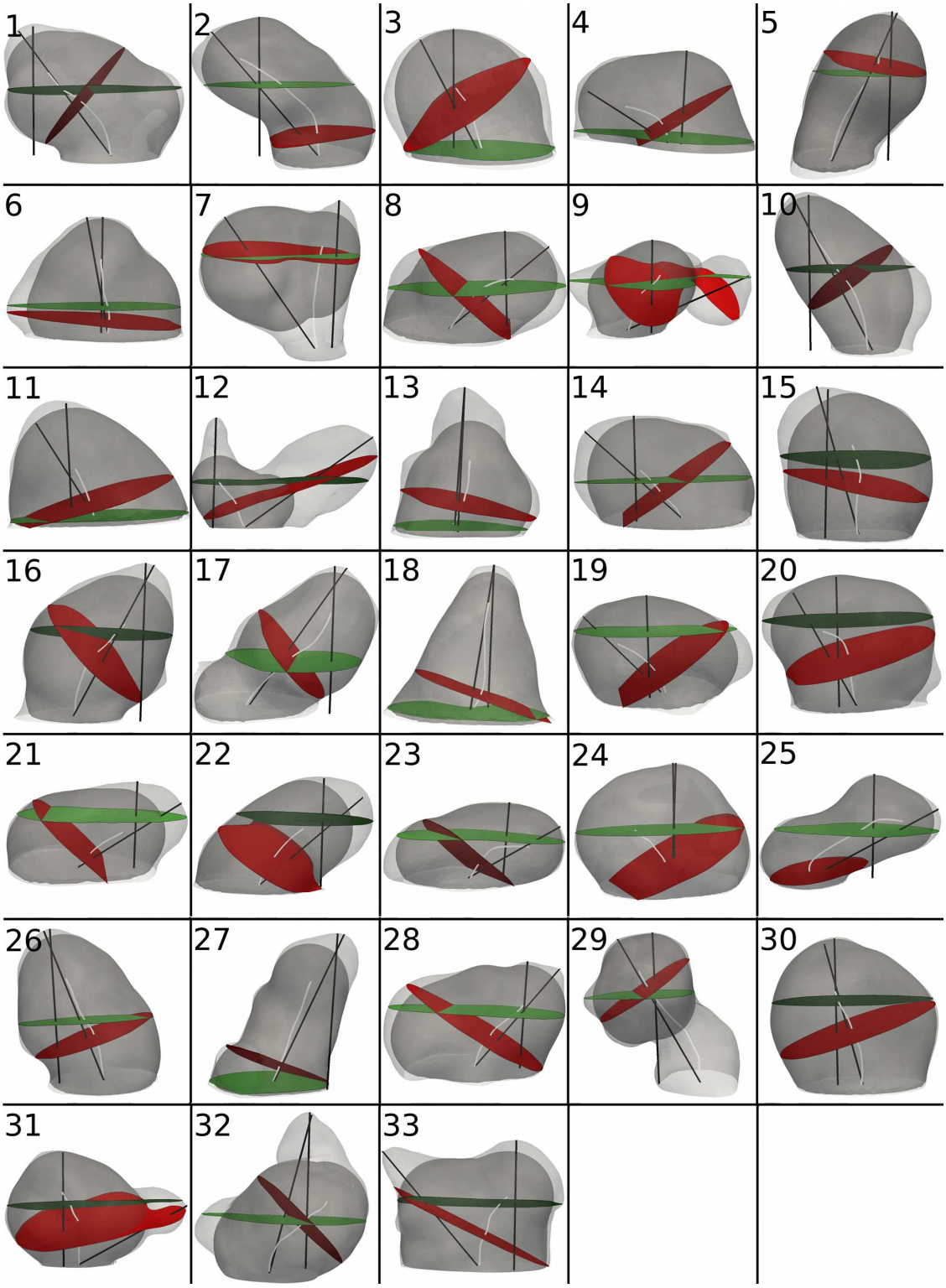
1
2
3
4
5
6
7
8
9
10
11
12
13
14
15
16
17
18
19
20
21
22
23
24
25
26
27
28
29
30
31
32
33

Figure 6.

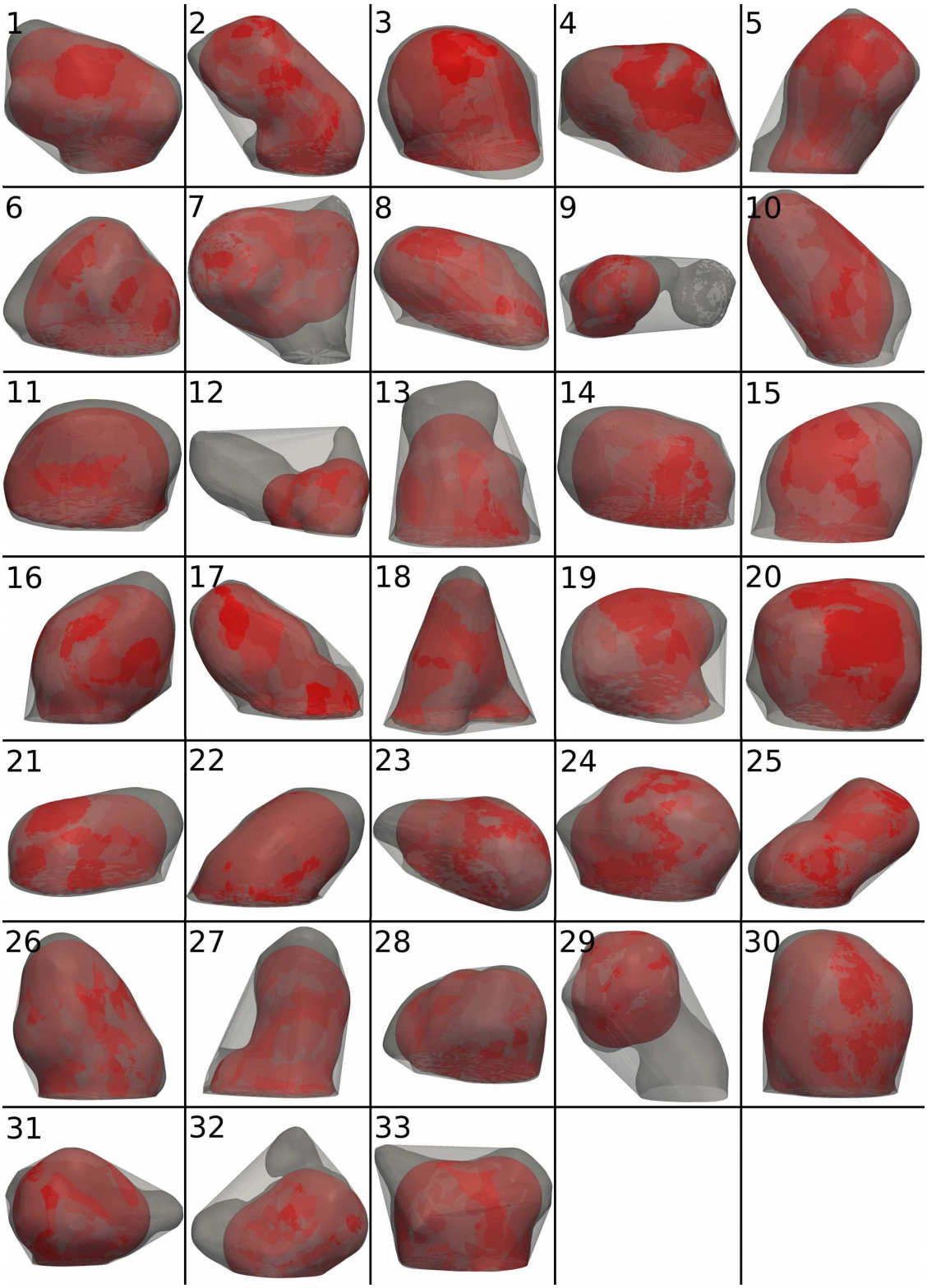
1
2
3
4
5
6
7
8
9
10
11
12
13
14
15
16
17
18
19
20
21
22
23
24
25
26
27
28
29
30
31
32
33

Figure 7.

Table 1. Descriptive statistics for geometry and derived variables on models segmented by operator 1 and 2 using level set and threshold methods.

	Variables	LS1 mean, std (min-max)	TH1 mean, std (min-max)	LS2 mean, std (min-max)	TH2 mean, std (min-max)
Ostium	ostium area	17.58, 12.97 (6.12 - 54.41)	17.34, 13.45 (5.16 - 53.34)	17.33, 13.05 (4.99 - 54.42)	17.41, 13.18 (4.99 - 51.64)
	ostium min size	1.77, 0.72 (0.62 - 3.74)	1.7, 0.71 (0.47 - 3.62)	1.73, 0.74 (0.21 - 3.64)	1.73, 0.71 (0.92 - 3.48)
	ostium max size	2.64, 0.91 (1.71 - 5.03)	2.76, 0.99 (1.72 - 5.39)	2.72, 0.96 (1.42 - 5.01)	2.72, 0.92 (1.47 - 4.65)
Sac	elipsoid saxis1	3.14, 1.10 (1.38 - 5.59)	3.17, 1.17 (1.44 -6.12)	3.12, 1.08 (1.39 - 5.57)	3.11, 1.13 (1.39 - 5.49)
	elipsoid saxis3	1.77, 0.67 (0.85 - 3.29)	1.78, 0.64 (0.88 - 3.29)	1.76, 0.67 (0.82 - 3.21)	1.78, 0.67 (0.53 - 3.23)
	sac surface area	115.8, 76.3 (25.6 - 288.9)	123.9, 81.4 (29.9 - 352.4)	120.4, 76.9 (28.4 - 296.4)	125.5, 79.4 (29.8 - 314.7)
	sac volume	109.2, 102.6 (9.6 - 337.9)	113.4, 107.1 (12.1 - 357.1)	110.5, 102.4 (10.4 - 339.5)	114.8, 107.1 (10.8 - 353.2)
	elipsoid volume	64.6, 62.2 (6.3 - 228.9)	65.1, 63.1 (7.5 - 232.2)	64.0, 61.5 (6.4 - 217.3)	65.8, 64.4 (5.13 - 235.8)
	sac largest section area	22.36, 16.74 (4.64 - 69.37)	21.62, 13.9 (7.1 - 53.16)	23.17, 18.0 (5.20 - 73.88)	22.15, 14.82 (4.63 - 55.26)
Core	sac centerline length	5.40, 1.96 (2.14 - 9.51)	5.65, 2.13 (2.11 - 9.93)	5.3, 1.98 (1.77 - 9.06)	5.56, 1.97 (2.16 - 9.58)
	VDC envelope surface area	98.8, 63.2 (24.3 - 244.1)	99.4, 63.2 (23.8 - 247.5)	97.3, 63.3 (20.4 - 237.3)	99.7, 64.1 (20.3 - 251.2)
	VDC envelope volume	93.0, 88.0 (9.1 - 323.3)	92.8, 87.6 (9.0 - 322.7)	90.7, 86.9 (7.3 - 309.2)	94.2, 88.9 (7.1 - 334.2)
Parent Vessel	vessel diameter	2.8, 0.96 (1.53 - 5.28)	2.56, 0.86 (1.36 - 4.87)	2.72,0.89 (1.53 - 5.31)	2.68, 0.93 (1.49 - 5.13)
Angulation	θ sac_vessel (LAT)	64, 27 (23 - 106)	74, 40 (16 - 159)	69, 29 (28 - 111)	67, 28 (21 - 111)
	θ neck_vessel (LAT)	70, 26 (17 - 115)	77, 37 (34 - 155)	74, 26 (40 - 123)	74, 26 (41 - 126)
	θ sac_vessel (TER)	21, 14 (0.1 - 42)	28, 16 (0.6 - 53)	25, 19 (0.7 - 71)	25, 15 (2 - 54)
	θ neck_vessel (TER)	22, 11 (2 - 42)	22, 14 (0.1 - 46)	21, 13 (1 - 49)	22, 11 (2 - 39)
Derived	aspect ratio	1.3, 0.46 (0.72 - 2.29)	1.48, 0.68 (0.76 - 3.66)	1.32, 0.51 (0.73 - 2.77)	1.44, 0.54 (0.82 - 2.75)
	size ratio	2.03, 0.76 (0.94 - 3.89)	2.35, 1.0 (0.89 - 4.78)	2.02, 0.72 (0.89 - 3.81)	2.21, 0.89 (1.09 - 4.63)

indexes	sac volume-to-ostium ratio	5.93, 4.25 (1.37 - 22.0)	6.76, 5.54 (1.61 - 29.38)	6.13, 4.13 (2.03 - 21.38)	6.39, 4.0 (2.05 -19.79)
	core volume-to-ostium ratio	5.05, 3.63 (1.30 - 18.76)	5.55, 4.62 (1.28 - 23.96)	4.97, 3.46 (1.46 - 17.07)	5.26, 3.43 (1.43 - 15.91)
	bottelenck factor	1.34, 0.77 (0.66 - 4.41)	1.44, 0.81 (0.72 - 4.71)	1.40, 0.75 (0.59 - 4.22)	1.41, 0.61 (0.62 - 3.11)
	ellipsoid axes ratio	0.58, 0.13 (0.28 - 0.82)	0.59, 0.16 (0.33 - 0.84)	0.58, 0.14 (0.30 - 0.85)	0.59, 0.15 (0.31 - 0.82)

VDC = Voronoi Diagram Core
LAT / TER = lateral / terminal
TH1,2 = models thresholded by operator 1 and 2
LS1,2 = models reconstructed with level sets by operator 1 and 2

Table 2. Interclass coefficients between different between different reconstruction techniques and operators, and relative errors of measurements obtained on thresholded models compared to those obtained on models segmented by way of a level set technique.

	Variables	Interclass Coefficient (ICC)				Relative Error (mean, std)			
		LS1 vs TH1	LS2 vs TH2	LS1 vs LS2	TH1 vs TH2	TH1 vs LS1	TH2 vs LS2	TH2 vd LS1	TH1 vs LS2
Ostium	ostium area	0.98	0.98	0.996	0.99	0.12, 0.11	0.14, 0.11	0.14, 0.12	0.15, 0.12
	ostium min size	0.97	0.95	0.99	0.97	0.09, 0.08	0.19, 0.57	0.10, 0.11	0.12, 0.2
	ostium max size	0.84	0.96	0.89	0.95	0.12, 0.21	0.09, 0.07	0.13, 0.19	0.11, 0.09
Sac	elipsoid saxis1	0.94	0.96	0.99	0.99	0.08, 0.09	0.07, 0.08	0.06, 0.09	0.07, 0.08
	elipsoid saxis3	0.97	0.94	0.98	0.96	0.09, 0.12	0.11, 0.15	0.10, 0.14	0.08, 0.12
	sac surface area	0.98	0.98	0.995	0.98	0.10, 0.09	0.11, 0.12	0.17, 0.15	0.07, 0.06
	sac volume	0.99	0.99	0.998	0.99	0.10, 0.10	0.12, 0.11	0.15, 0.14	0.08, 0.07
	elipsoid volume	0.997	0.99	0.998	0.99	0.10, 0.11	0.12, 0.14	0.12, 0.13	0.09, 0.12
	sac largest section area	0.93	0.90	0.99	0.98	0.15, 0.18	0.13, 0.15	0.13, 0.12	0.18, 0.18
Core	sac centerline length	0.97	0.91	0.94	0.96	0.07, 0.07	0.11, 0.18	0.07, 0.08	0.10, 0.17
	VDC envelope surface area	0.99	0.995	0.997	0.99	0.07, 0.06	0.07, 0.09	0.08, 0.07	0.08, 0.09
	VDC envelope volume	0.99	0.995	0.997	0.99	0.09, 0.08	0.11, 0.16	0.11, 0.10	0.11, 0.11
Parent Vessel	vessel diameter	0.87	0.96	0.96	0.92	0.10, 0.09	0.08, 0.06	0.08, 0.06	0.09, 0.08
Angulation	θ sac_vessel (LAT)	0.73	0.91	0.88	0.71	0.29, 0.33	0.14, 0.12	0.22, 0.37	0.28, 0.50
	θ neck_vessel (LAT)	0.64	0.91	0.85	0.80	0.28, 0.35	0.11, 0.11	0.27, 0.38	0.22, 0.26
	θ sac_vessel (TER)	0.33	0.40	0.71	0.78	2.1, 4.2	3.1, 6.7	2.6, 4.6	3.1, 6.1
	θ neck_vessel (TER)	0.73	0.62	0.64	0.89	0.52, 0.64	0.56, 0.43	0.39, 0.47	0.79, 0.78

Derived indexes	aspect ratio	0.84	0.84	0.89	0.93	0.14, 0.13	0.14,0.21	0.12, 0.12	0.15, 0.21
	size ratio	0.81	0.73	0.91	0.90	0.19, 0.17	0.18, 0.28	0.14, 0.12	0.18, 0.27
	sac volume-to-ostium ratio	0.94	0.97	0.99	0.92	0.15, 0.13	0.12, 0.1	0.17, 0.18	0.11, 0.1
	core volume-to-ostium ratio	0.96	0.98	0.99	0.93	0.12, 0.11	0.15, 0.16	0.12, 0.12	0.15, 0.16
	bottleneck factor	0.85	0.81	0.97	0.80	0.18, 0.18	0.17, 0.19	0.20,0.22	0.19, 0.19
	ellipsoid axes ratio	0.63	0.58	0.89	0.78	0.16, 0.35	0.17, 0.32	0.16, 0.35	0.16, 0.30

VDC = Voronoi Diagram Core

LAT / TER = lateral / terminal

TH1,2 = models thresholded by operator 1 and 2

LS1,2 = models reconstructed with level sets by operator 1 and 2

Table 3. Numerical values for geometric parameters depicted in Picture 6 and 7

case	max an. height (mm)	max perp height (mm)	sac cl length (mm)	perp c.s. area (mm^2)	cl c.s. area (mm^2)	c.h. vol (mm^3)	VDC vo (mm^3)
01	7.0	5.8	6.6	34.4	21.8	136.6	111.7
02	7.8	6.7	8.2	24.2	18.5	127.0	112.3
03	2.6	2.5	2.5	6.8	6.2	13.7	11.6
04	2.3	1.8	2.1	7.0	4.6	9.2	9.1
05	5.2	4.9	5.4	11.2	9.8	40.9	36.6
06	6.1	6.0	5.4	38.6	39.0	159.4	148.2
07	8.5	7.8	7.5	39.4	38.8	207.2	165.1
08	3.8	2.9	3.8	13.7	9.5	30.8	27.2
09	8.2	4.4	5.0	30.8	27.9	117.0	55.4
10	6.5	6.0	6.5	15.1	12.9	65.3	58.9
11	2.8	2.6	2.7	11.9	11.2	21.8	19.8
12	11.6	8.0	6.0	60.5	69.4	340.6	132.6
13	9.8	9.8	7.4	54.2	51.8	349.3	272.6
14	7.2	5.7	6.4	59.5	46.7	260.8	236.9
15	3.3	3.0	3.2	7.7	7.6	17.7	16.2
16	8.9	8.1	8.5	51.5	47.2	295.0	274.6
17	5.6	4.7	5.7	13.7	9.7	49.0	41.9
18	4.7	4.7	4.3	11.6	8.6	26.0	24.3
19	3.4	2.9	3.5	14.1	10.2	31.5	27.9
20	4.7	4.5	4.9	20.8	19.7	73.6	68.6
21	3.6	2.6	3.0	13.8	9.3	28.3	24.4
22	4.2	3.3	3.7	14.5	11.2	36.9	25.2
23	3.4	2.5	3.5	14.1	7.6	26.4	24.0
24	5.8	5.8	5.6	43.6	37.8	185.1	178.1
25	7.9	5.8	8.2	34.1	20.2	130.7	120.6
26	9.9	9.5	9.5	49.2	44.9	338.9	323.3
27	7.4	6.9	6.8	21.4	17.7	104.5	85.9
28	5.0	4.2	4.9	24.6	22.0	79.7	72.9
29	6.8	6.3	6.9	13.0	14.2	73.5	37.0
30	4.4	4.3	4.5	15.2	14.6	48.2	46.6
31	8.6	7.6	7.7	67.7	66.13	360.2	310.9
32	16.5	15.8	11.8	139.8	98.0	1358.3	947.0
33	9.2	7.2	7.3	57.1	61.6	336.9	290.6

max an height = maximum aneurysm height

max perp height =maximum perpendicular height

sac cl length = sac centerline length

perp c.s area = maximum sac area along perpendilar direction

cl c.s. area = maximum area along centerline tangent directior

c.h.vol = convex hull volume

VDC vol = Voronoi Diagram Core volume

Table 4. Descriptive statistics of straight-line parameters on models segmented by operators 1 and 2 using level set (LS) and threshold (TH) methods.

Variables	LS1 mean, std (min-max)	TH1 mean, std (min-max)	LS2 mean, std (min-max)	TH2 mean, std (min-max)
maximum aneurysm height	5.9, 2.4 (2.3 - 11.6)	6.4, 2.4 (2.7 - 11.8)	6.0, 2.3 (2.4 - 11.6)	6.2, 2.3 (2.7 - 11.6)
maximum perpendicular height	5.1, 2.1 (1.8 - 9.8)	5.5, 2.3 (2.0 - 10.1)	5.2, 2.0 (2.0 - 9.8)	2.3, 2.0 (2.0 - 9.3)
convex hull surface area	102.0, 70.0 (18.8 - 290.8)	113.4, 72.0 (22.9 - 327.0)	104.9, 70.8 (20.0 - 305.0)	110.8, 73.6 (21.4 - 307.0)
convex hull volume	114.1, 106.7 (9.2 - 349.3)	125.9, 118.4 (12.0 - 478.6)	118.9, 112.4 (9.7 - 418.9)	125.4, 118.7 (10.2 - 431.8)
non sphericity index	0.16, 0.08 (0.03 - 0.38)	0.21, 0.09 (0.03 - 0.42)	0.20, 0.08 (0.08 - 0.43)	0.23, 0.08 (0.09 - 0.42)
ellipticity index	0.17, 0.07 (0.08 - 0.36)	0.21, 0.09 (0.07 - 0.45)	0.18, 0.07 (0.08 - 0.36)	0.20, 0.07 (0.09 - 0.38)
undulation index	0.04, 0.05 (0.0002 - 0.21)	0.11, 0.10 (0.002 - 0.38)	0.06, 0.07 (0.001 - 0.28)	0.07, 0.09 (0.003 - 0.47)
aspect ratio	1.21, 0.43 (0.66 - 2.38)	1.45, 0.78 (0.68 - 4.51)	1.28, 0.44 (0.72 - 2.49)	1.34, 0.46 (0.76, 2.44)
bottleneck factor	1.19, 0.22 (1.0 - 1.99)	1.28, 0.31 (1.0 - 2.58)	1.22, 0.23 (1.0 - 2.06)	1.26, 0.24 (0.99 - 2.04)

aspect ratio = maximum perpendicular height/ostium diameter
bottleneck factor = maximum diameter/ostium diameter

Table 5. Interclass coefficients for straight-line parameters between different reconstruction techniques and operators; relative errors of measurements obtained on thresholded subsets compared to those performed on models segmented by means of a level set technique.

Variables	Interclass Coefficient (ICC)				Relative Error (mean, std)			
	LS1 vs TH1	LS2 vs TH2	LS1 vs LS2	TH1 vs TH2	TH1 vs LS1	TH2 vs LS2	TH2 vd LS1	TH1 vs LS2
maximum aneurysm height	0.93	0.97	0.99	0.93	0.11, 0.15	0.07, 0.09	0.09, 0.12	0.09, 0.13
maximum perpendicular height	0.93	0.98	0.98	0.9	0.09, 0.13	0.05, 0.05	0.08, 0.06	0.07, 0.11
convex hull surface area	0.97	0.99	0.99	0.97	0.18, 0.21	0.11, 0.11	0.15, 0.12	0.14, 0.17
convex hull volume	0.97	0.99	0.99	0.99	0.18, 0.18	0.12, 0.11	0.17, 0.14	0.14, 0.12
non sphericity index	0.73	0.73	0.80	0.60	0.51, 0.66	0.23, 0.19	0.68,0.82	0.20, 0.18
ellipticity index	0.67	0.85	0.96	0.80	0.27, 0.28	0.16, 0.18	0.23, 0.23	0.20, 0.25
undulation index	0.20	0.74	0.81	0.39	15.2, 62.0	2.3, 4.8	3.0, 6.7	4.1, 8.7
aspect ratio	0.69	0.93	0.96	0.77	0.17, 0.21	0.08, 0.08	0.13, 0.11	0.12,0.17
bottleneck factor	0.86	0.89	0.94	0.90	0.07, 0.07	0.06, 0.07	0.06, 0.08	0.06, 0.06

aspect ratio = maximum perpendicular height/ostium diameter
bottleneck factor = maximum diameter/ostium diameter